Supporting Information

Triazine-Functionalized Donor−π−Acceptor Covalent−Organic Frameworks with Oligo(Phenylenevinylene) Bridge for Efficient Photocatalytic H_2O_2 Evolution

Jie Fan,[a,c] Shiguang Lv,[a,b] Yayu Yan,[a,c] Qiaohong Li,[*a,c] Shao-Xia Lin[*a,c,d] and Daqiang Yuan[*a,c,d]

[a] State Key Lab of Structure Chemistry, Fujian Institute of Research on the Structure of Matter, Chinese Academy of Sciences, Fuzhou, Fujian, 350002, China.

[b.] Fujian Normal University, Fuzhou, Fujian, 350007, China.

[c.] University of Chinese Academy of Sciences, Beijing, 100049, China.

[d.] Fujian Science and Technology Innovation Laboratory for Optoelectronic Information of China, Fuzhou 350108, China.

1. Materials and Synthesis

1.1 Materials

All solvents and starting materials obtained from commercial sources were used without further purification. 1,4-Dioxane, acetone, trifluoroacetic acid, acetic acid, methanol, sodium sulfate, and a 30% H_2O_2 stock solution were purchased from Sinopharm Chemical Reagent Co., Ltd. (Shanghai, China). 1,3,5-Tris(4-aminophenyl)benzene (TAPB) and tris(4-aminophenyl)amine (TAPA) were obtained from MERYER (Shanghai, China). Potassium titanium oxalate was supplied by Leyan (Shanghai, China), and mesitylene was acquired from Macklin (Shanghai, China). 4,4',4''-(1,3,5-Triazine-2,4,6-triyl)trianiline (TAPT), 1,3,5-tris(bromomethyl)benzene, potassium tert-butoxide, triethyl phosphite, benzyl alcohol, terephthalaldehyde, and 5,5-dimethyl-1-pyrroline N-oxide (DMPO) were purchased from Titan (Shanghai, China). Other chemical reagents were supplied by local chemical suppliers.

1.2 Synthesis of 1,3,5-tris (*p*-formylstyrene) benzene (OPV-CHO) Monomer

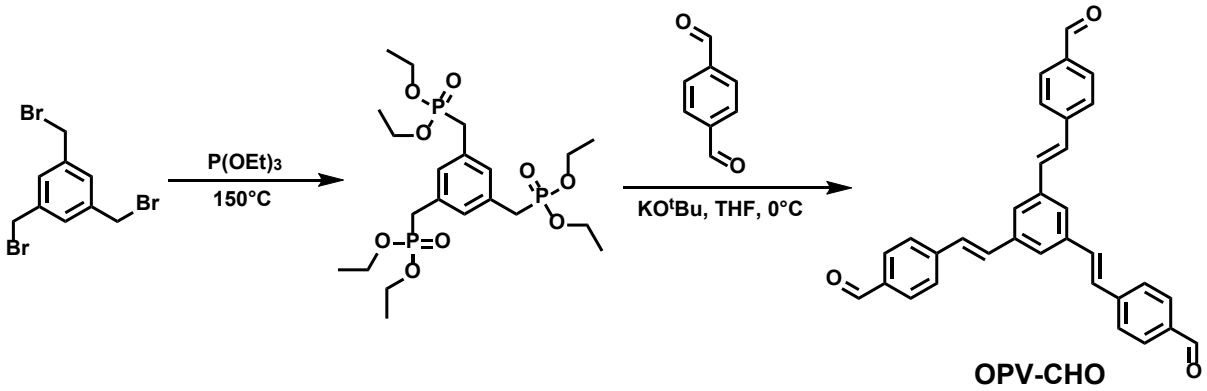

Scheme S1. Synthetic route to the OPV-CHO monomer

1.2.1 Synthesis of 1,3,5-Tris(diethyl methylphosphonate)benzene

1,3,5-Tris(diethyl methylphosphonate)benzene was synthesized according to a previously reported method.[1] In a typical procedure, 1,3,5-tris(bromomethyl)benzene (1.5 g, 4.2 mmol) and triethyl phosphite (30 mL, 181.2 mmol) were added to a 100 mL single-necked flask under a nitrogen atmosphere. The mixture was heated at 150 °C for 4 hours. After cooling to room temperature, the excess triethyl phosphite was removed under reduced pressure. The system was then placed under vacuum until no more liquid droplets were observed condensing at the

upper end of the condenser, yielding the title compound as a yellow oil.

1.2.2 Synthesis of 1,3,5-Tris(*p*-formylstyryl)benzene (OPV-CHO)

1,3,5-Tris(*p*-formylstyryl)benzene was synthesized according to a previously reported method.[1] Under a nitrogen atmosphere, a mixture of 1,3,5-tris(diethylmethylphosphonate)benzene (2.9 g, 5.49 mmol), *p*-benzaldehyde (6.62 g, 49.4 mmol), and THF (220 mL) was placed in a two-necked flask immersed in an ice-water bath and stirred for 30 minutes. Potassium *tert*-butoxide (3.5 g, 31.25 mmol) was then added, and the reaction mixture was allowed to warm to room temperature and stirred overnight. The reaction was quenched by adding 100 mL of water, and the pH was adjusted to approximately 2 with 1 M HCl (20 mL), followed by an additional 2 hours of stirring. THF was removed by rotary evaporation. The resulting precipitate was collected by natural filtration, washed successively with water and methanol (three times each), and dried under vacuum at 40 °C to afford the product as a yellow solid (0.80 g, 31% yield). ^{1}H NMR (400 MHz, $(CD_3)_2SO$, ppm): δ = 7.56 (s, 6H), 7.88 (d, 6H), 7.93 (s, 3H), 7.96 (d, 6H), 10.02 (s, 3H). ^{13}C NMR (400 MHz, $(CD_3)_2SO$, ppm): δ = 192.9, δ =143.4, δ =138.0, δ =135.6, δ =131.8, δ =130.6, δ =128.8, δ =127.6, δ = 125.8.

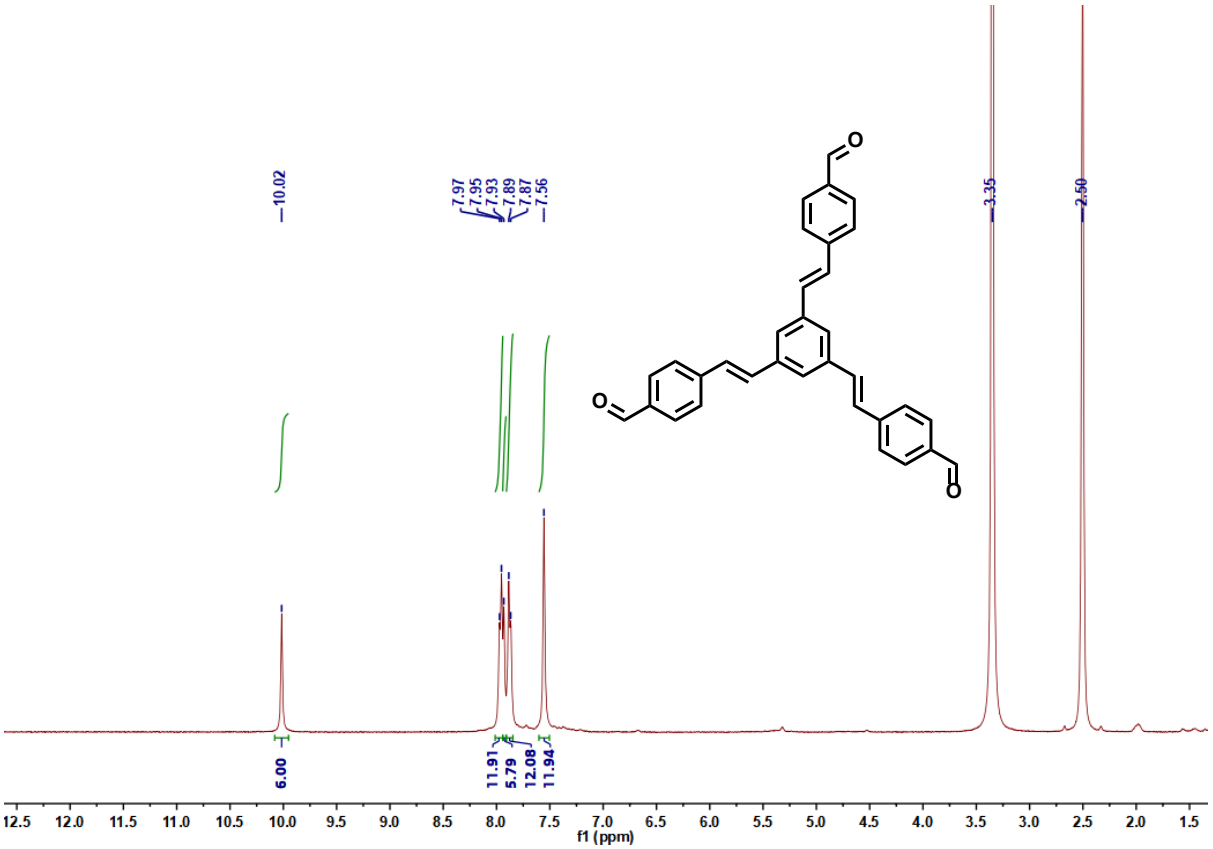

Figure S1. ^{1}H-NMR spectrum of 1,3,5-Tris(*p*-formylstyryl)benzene.

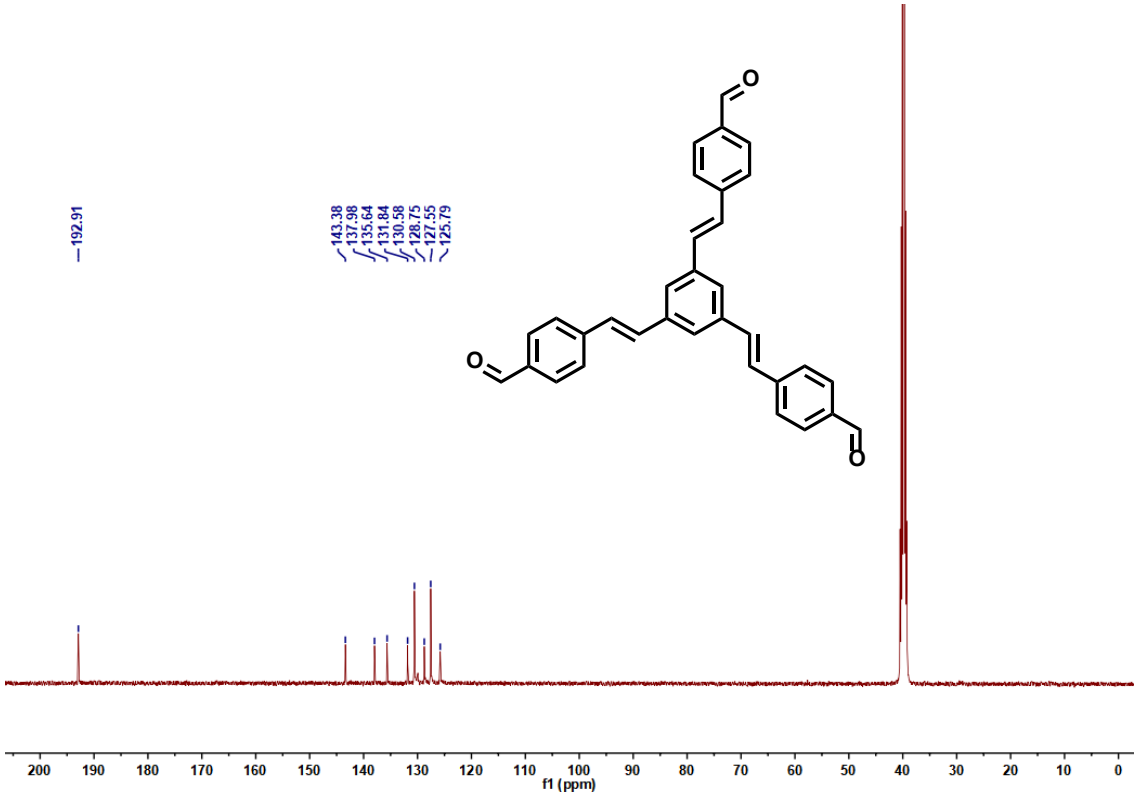

Figure S2. ^{13}C-NMR spectrum of 1,3,5-Tris(*p*-formylstyryl)benzene.

1.3 Synthesis of OPV-TAPT-COF

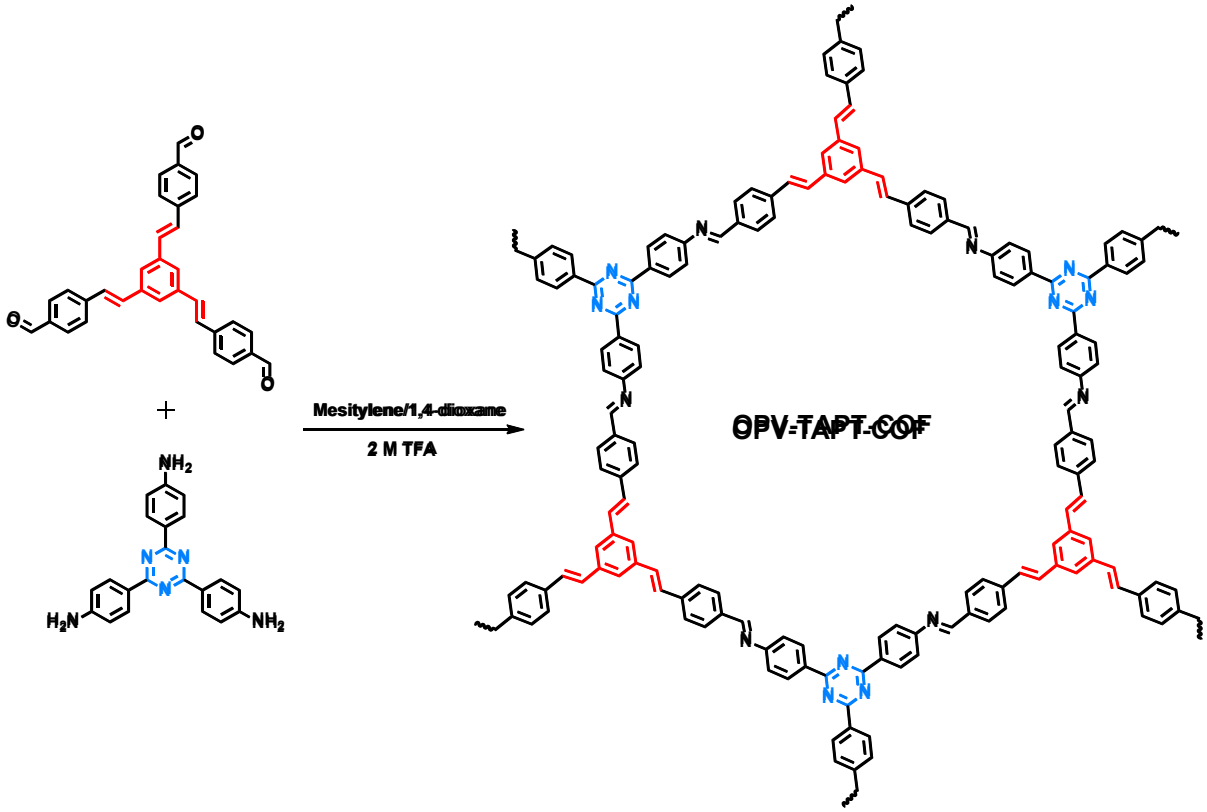

Scheme S2. Synthesis of OPV-TAPT-COF.

A mixture of TAPT (7 mg, 0.02 mmol), OPV-CHO (9.4 mg, 0.02 mmol), mesitylene (0.7 mL), and 1,4-dioxane (0.3 mL) was added to a 20 mL Pyrex tube and sonicated for 10 minutes to afford a homogeneous suspension. Trifluoroacetic acid (2 M, 0.1 mL) was then added to the mixture. The tube was flash-frozen in a liquid nitrogen bath and degassed though three freeze-pump-thaw cycles. After being sealed under vacuum, the tube was heated at 120 °C for 3 days. The resulting precipitate was collected by filtration, thoroughly washed with acetone, and dried overnight in a vacuum oven at 65 °C to yield OPV-TAPT-COF as a dark red powder.

1.4 Synthesis of OPV-TAPB-COF

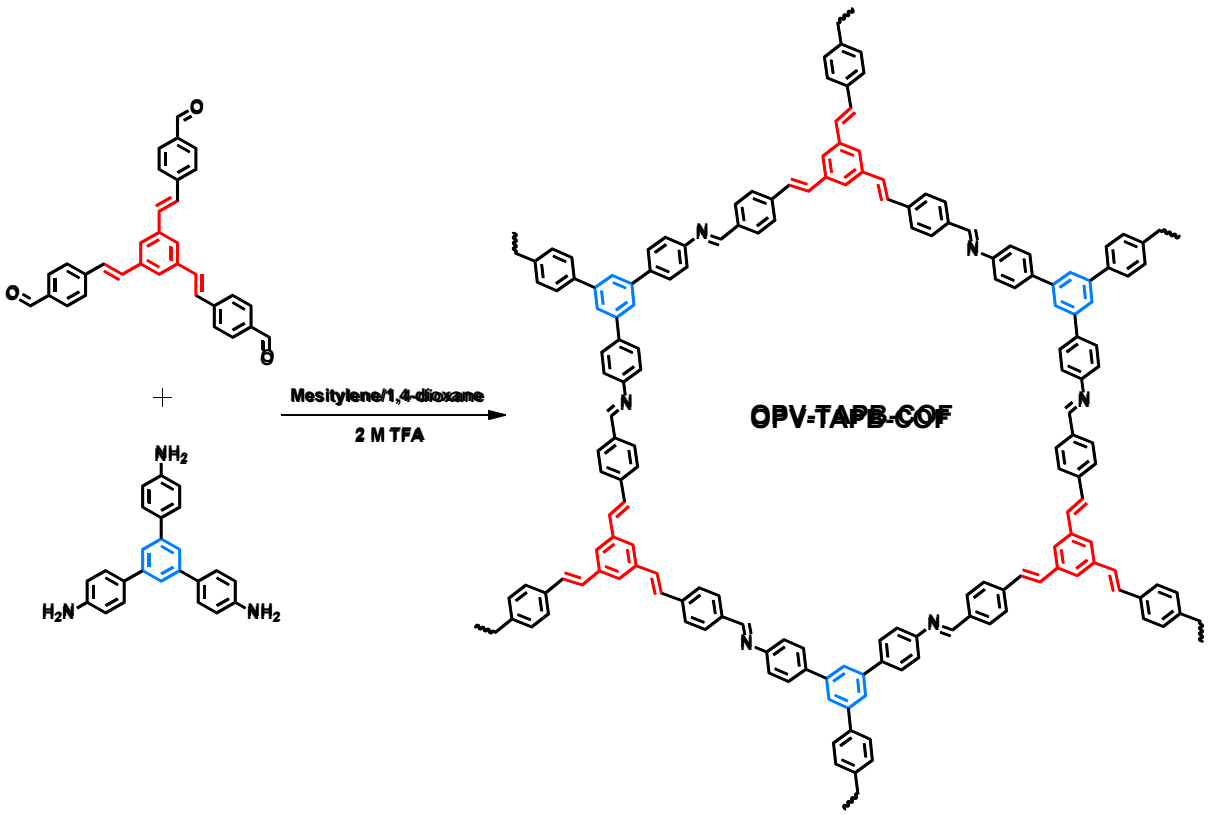

Scheme S3. Synthesis of OPV-TAPB-COF.

A mixture of TAPB (7 mg, 0.02 mmol), OPV-CHO (9.4 mg, 0.02 mmol), mesitylene (0.7 mL), and 1,4-dioxane (0.3 mL) was added to a 20 mL Pyrex tube and sonicated for 10 minutes to afford a homogeneous suspension. Trifluoroacetic acid (2 M, 0.1 mL) was then added to the mixture. The tube was flash-frozen in a liquid nitrogen bath and degassed though three freeze-pump-thaw cycles. After being sealed under vacuum, the tube was heated at 120 °C for 3 days. The resulting precipitate was collected by filtration, thoroughly washed with acetone, and dried overnight in a vacuum oven at 65 °C to yield OPV-TAPT-COF as a dark red powder.

1.5 Synthesis of OPV-TAPA-COF

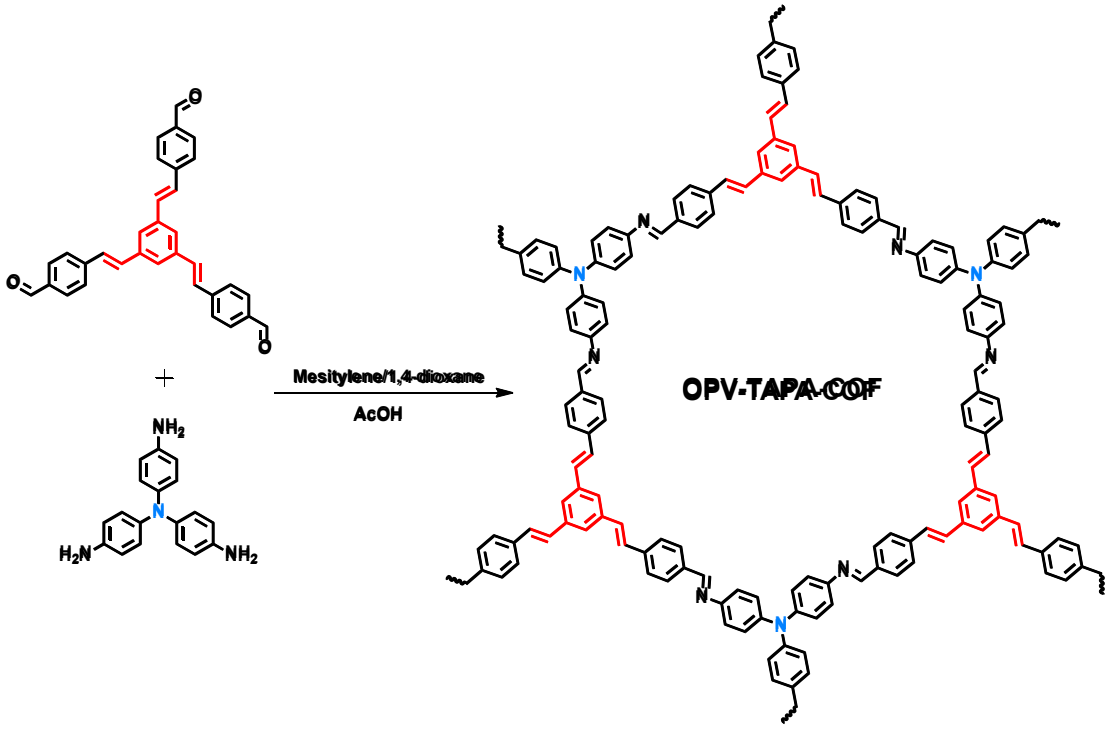

Scheme S4. Synthesis of OPV-TAPA-COF.

A mixture of TAPA (6 mg, 0.02 mmol), OPV-CHO (9.4 mg, 0.02 mmol), mesitylene (0.7 mL), and 1,4-dioxane (0.3 mL) was added to a 20 mL Pyrex tube and sonicated for 10 minutes to afford a homogeneous suspension. acetic acid (0.1 mL) was then added to the mixture. The tube was flash-frozen in a liquid nitrogen bath and degassed though three freeze-pump-thaw cycles. After being sealed under vacuum, the tube was heated at 120 °C for 3 days. The resulting precipitate was collected by filtration, thoroughly washed with acetone, and dried overnight in a vacuum oven at 65 °C to yield OPV-TAPT-COF as a tan powder.

2.Characterizations

2.1 Powder X-ray Diffraction (PXRD)

The powder X-ray diffraction (PXRD) patterns were collected on a D/max 2500 VL/PC X-ray diffractometer (Rigaku SmartLab, Japan) with Cu Kα radiation (λ = 1.5406 Å) at 45 kV, 200 mA. Diffraction intensity data for 2θ from 2~40° were collected at the scanning speed of 10 deg/min with 2θ step increment of 0.01°.

2.2 Fourier-Transform Infrared (FT-IR) Spectroscopy

Fourier-transform infrared (FT-IR) spectra of the starting materials and COF samples were recorded on a Vertex70 spectrometer.

2.3 Scanning Electron Microscopy (SEM)

The surface morphology of the COFs was characterized using a scanning electron microscope (SEM, Thermo Fisher Apreo 2S HiVac) at an acceleration voltage of 10 kV.

2.4 Field Emission Transmission Electron Microscopy (FE-TEM)

FE-TEM images were obtained on a Talos-F200X microscopy at an accelerating voltage of 200 kV.

2.5 X-ray Photoelectron Spectroscopy (XPS)

X-ray photoelectron spectroscopy (XPS) measurements were performed on a Thermo Scientific Escalab 250Xi instrument equipped with an Al Kα micro-focused X-ray source. All binding energies were calibrated with reference to the C 1s peak at 284.6 eV.

2.6 Solid Ultraviolet-Visible Spectroscopy (Solid UV-DRS)

The solid-state UV-vis absorption spectra of the monomers and the COFs were recorded using a PerkinElmer Lambda 950 UV-Vis spectrophotometer.

2.7 Photoelectrochemical (PEC) Characterizations

The photoelectrochemical (PEC) measurements were performed using photoelectrodes prepared from the sample powders. The electrodes were fabricated via a drop-coating method. Briefly, 5 mg of the powder was dispersed in a solution containing 950 μL of ethanol and 50 μL of a 5 wt% Nafion solution. The resulting slurry was sonicated for 30 minutes to form a homogeneous dispersion, which was then drop-cast onto a piece of fluorine-doped tin oxide (FTO) glass and dried to serve as the working electrode. The PEC measurements were conducted in a standard three-electrode configuration using an electrochemical workstation (CHI 660E), with the prepared photoelectrode, a Pt wire, and an Ag/AgCl electrode acting as the working, counter, and reference electrodes, respectively. A 0.2 M Na_2SO_4 aqueous solution

(pH = 7) was used as the electrolyte. Transient photocurrent responses were measured under intermittent irradiation from a 300 W Xe lamp. Mott-Schottky plots were recorded in a potential range from -1 to 1 V (vs. Ag/AgCl).

2.8 Steady-State Photoluminescence (PL) and Time-Resolved Photoluminescence (TRPL) Measurements

Steady-state photoluminescence (PL) and time-resolved photoluminescence (TRPL) spectra of the three COFs were acquired using an Edinburgh Instruments FLS1000 spectrophotometer.

2.9 Liquid-State Nuclear Magnetic Resonance (NMR)

The ^{1}H and ^{13}C NMR spectra were recorded on a Bruker AVANCE III 400 spectrometer operating at 400 MHz.

2.10 Solid-State ^{13}C NMR Spectroscopy

Solid-state ^{13}C cross-polarization magic-angle spinning (CP/MAS) NMR spectra were acquired on a Bruker AVANCE 400 spectrometer operating at 400 MHz.

2.11 Brunauer-Emmett-Teller (BET) Surface Area

Nitrogen adsorption–desorption isotherms were measured at 77 K using a Beishide BSD-660M analyzer, from which the BET specific surface areas were derived.

2.12 Thermogravimetric Analysis (TGA)

Thermogravimetric analysis was performed on a NETZSCH STA 449F3 instrument under a nitrogen atmosphere.

3. Photocatalytic H_2O_2 Production

The COF photocatalyst (3 mg) was dispersed in deionized water (30 mL) within a 50 mL sealed glass vial by sonication for 15 minutes to form a homogeneous suspension. The resulting dispersion was then purged with O_2 in the dark under stirring for 15 minutes at a flow rate of 100 mL/min to achieve oxygen saturation. The resulting dispersion was irradiated at $\lambda > 420$nm

using a 300 W Xe lamp (PLS-SXE300, Beijing Perfect light).

3. 1 H_2O_2 Detection Methods

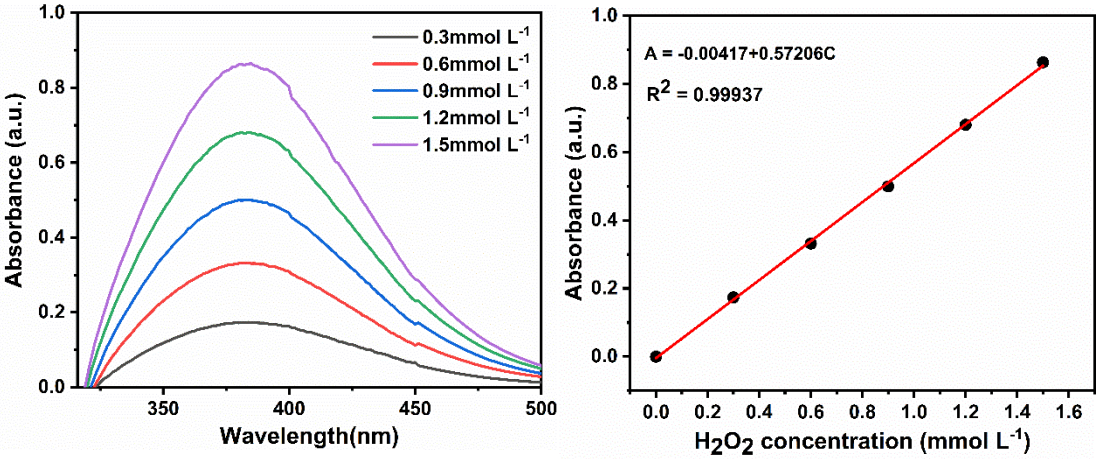

During the irradiation, reaction aliquots (1.2 mL) were sampled at 15-minute intervals using a syringe. The samples were immediately filtered through a 0.22 μm membrane to separate the photocatalyst. The concentration of H_2O_2 in the filtrate was quantified by the potassium titanium oxalate method. Briefly, in an acidic medium, H_2O_2 reacts with titanium ions to form a stable orange complex.[2] The filtrate was mixed with a colorimetric reagent (0.02 M potassium titanium oxalate, pH = 4) in a 1:1 volume ratio. After standing for 8 minutes, the absorbance of the mixture was measured at 384 nm using a UV/Vis spectrophotometer. The H_2O_2 concentration was calculated from a pre-established linear calibration curve (0.3–1.6 mM) relating absorbance to the concentration of standard H_2O_2 solutions.

3.2 Long-Term Performance Testing

The sampling and analysis of H_2O_2 were performed as described previously, except that the sampling interval was set to 1 hour.

3.3 Measurement of Apparent Quantum Yield

The apparent quantum yield (AQY) was measured according to a method adapted from the literature. The photocatalytic reaction was conducted using the photocatalyst (10 mg) dispersed in deionized water (15 mL) after sonication and O_2 purging. The system was irradiated with

light from a 300 W Xe lamp (PLS-SXE300D, Beijing Perfectlight) using bandpass filters at 420, 475, 500, 550, and 600 nm. The irradiation area of the reactor was approximately 2 cm^2. The light intensity at each wavelength was averaged from measurements at five representative points using a PL-MW2000 optical power meter (Beijing Perfectlight) and was determined to be, for instance, 10.5 mW cm^{-2} at 420 nm. The AQY was then calculated using the following equation:

$$AQY = \frac{(\text{number of } H_2O_2 \text{ production}) \times 2}{\text{number of incident photons}} \times 100\% \qquad \text{Equation-(1)}$$

4. Investigation into the Mechanism of Photocatalysis

4.1 Electron Paramagnetic Resonance (EPR) Measurement

Electron paramagnetic resonance (EPR) spectroscopy was employed to detect the superoxide radical ($\bullet O_2^-$) using 5,5-dimethyl-1-pyrroline N-oxide (DMPO) as the spin-trapping agent. The measurements were performed on a Bruker ELEXSYS-II E500 CW-EPR spectrometer. Briefly, the catalyst (5 mg) was dispersed in a methanol/water mixture (9:1 v/v, 1 mL) containing DMPO (0.2 mM) in a centrifuge tube. The dispersion was purged with O_2 for 10 minutes prior to irradiation. Subsequently, the supernatant was extracted after centrifugation, loaded into a one-end-sealed capillary tube, and this capillary was then inserted into a heat-resistant glass tube. The glass tube was finally sealed with a rubber septum. A Xe lamp ($\lambda > 420$ nm) served as the light source for irradiation.

4.2 Rotating-Disk Electrode (RDE) Measurement

A glassy carbon rotating disk electrode (PINE Research Instrumentation, USA) was used as the substrate for the working electrode. The working electrode was prepared as follows: COF powder (5 mg) was dispersed in a mixture of ethanol (0.45 mL) and Nafion solution (50 μL) by ultrasonication to form a homogeneous ink. Then, 20 μL of the resulting ink was drop-cast onto the electrode surface and dried at room temperature. Linear sweep voltammetry (LSV) was conducted in an O_2-saturated 0.1 M phosphate buffer solution (pH = 7) at a scan rate of 10 mV s^{-1} under various rotation rates. During the measurements, the electrode was vertically

illuminated by a Xe lamp to obtain photoelectrochemical kinetic data and information on peroxide formation. The average number of electrons (n) has been calculated by the Koutecky-Levich equation:

$$\frac{1}{J} = \frac{1}{J_L} + \frac{1}{J_K} = \frac{1}{B\omega^{1/2}} + \frac{1}{J_K} \quad \text{Equation-(2)}$$

$$B = 0.62nFC_0D_0^{2/3}V^{-1/6} \quad \text{Equation-(3)}$$

Where J is the measured current density, J_K and J_L are the kinetic and diffusion-limiting current densities, ω is the rotating speed (rad s^{-1}), n is transferred electron number, F is Faraday constant (96485 C mol^{-1}), C_0 is the bulk concentration of O_2 (1.26×10^{-3} mol cm^{-3}), D_0 is the diffusion coefficient of O_2 in 0.1 M phosphate buffer solution (2.7×10^{-5} cm^2 s^{-1}), and ν is kinetic viscosity of the electrolyte (0.01 cm^2 s^{-1}), respectively.

4.3 In-situ Diffuse Reflectance Infrared Fourier Transform (In-situ DRIFT) Spectroscopy

The experiments were conducted using a Thermo Fisher Nicolet 6700 spectrometer. Approximately 10 mg of catalyst was loaded into a dedicated in situ IR cell to ensure optimal signal intensity. The reaction gases (O_2 and H_2O vapor) were introduced into the cell through its CaF_2 window via an integrated fiber-optic light source (FX300, Beijing Perfect Light Technology Co., Ltd.). After collecting a background spectrum, O_2 was introduced at room temperature. The sample was then irradiated under constrained illumination using a 300 W Xe lamp equipped with a 420 nm cutoff filter. Spectra were acquired at 5, 10, 15, 20, and 30 minutes of illumination to capture the dynamic evolution of surface intermediates.

5. Computational Chemistry

5.1 Structural Simulation

The initial unit cells of OPV-TAPT-COF, OPV-TAPB-COF, and OPV-TAPA-COF were constructed using Materials Studio. The theoretical lattice parameters were used to define the initial cell dimensions, and the atomic positions were fully optimized by energy minimization

using the Forcite module. The fractional atomic coordinates of the resulting optimized crystal structures are provided in Supplementary Tables S2, S3, and S4.

5.2 DFT

Herein, all the calculation contents are based on the DFT theory and were completed using the Gaussian 16 software.[3] The structure optimization of COFs was performed using the B3LYP functional and the 6-31G(d,p) basis set, while TDDFT calculations were carried out using cam-B3LYP and aug-cc-pvdz basis sets, with Grimme's D3 dispersion correction included.[4-8] The calculating datas were analyzed and visualized using the Multiwfn program[9] and VMD software.[10]

6. Supplementary Figures

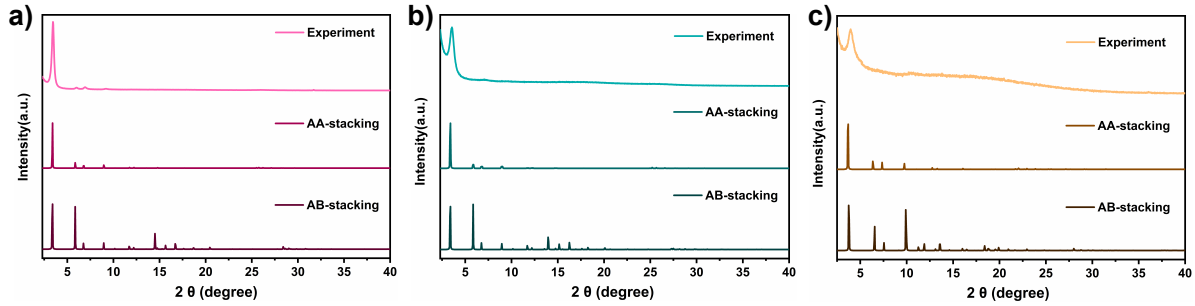

Figure S3. Experimental and simulated PXRD patterns for a) OPV-TAPT-COF, b) OPV-TAPB-COF, and c) OPV-TAPA-COF with AA and AB stacking models.

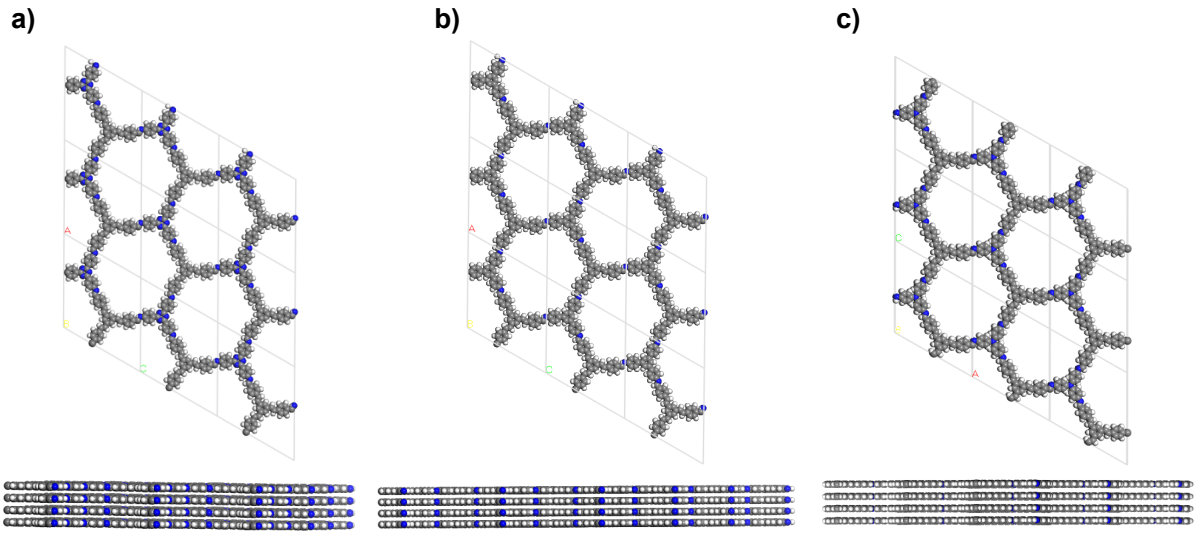

Figure S4. Top and side views for AA stacking model of a) OPV-TAPT-COF, b) OPV-TAPB-COF, and c) OPV-TAPA-COF.

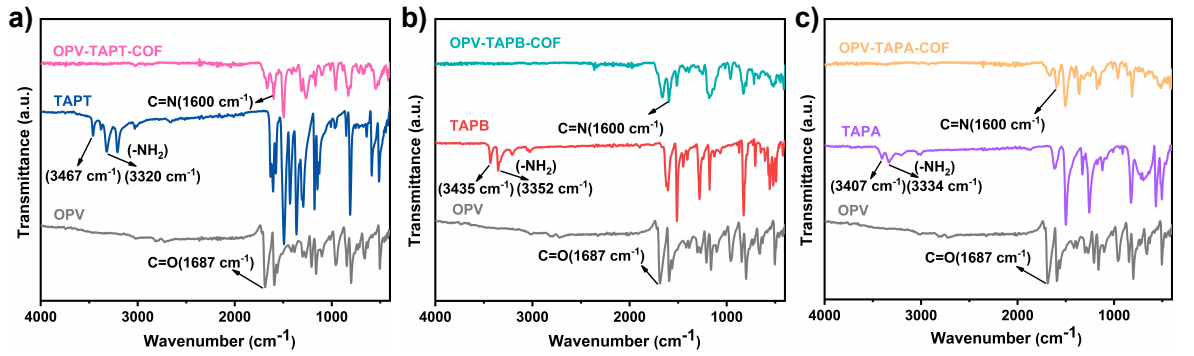

Figure S5. FT-IR spectra of a) OPV-TAPT-COF, b) OPV-TAPB-COF, c) OPV-TAPA-COF and their corresponding monomers.

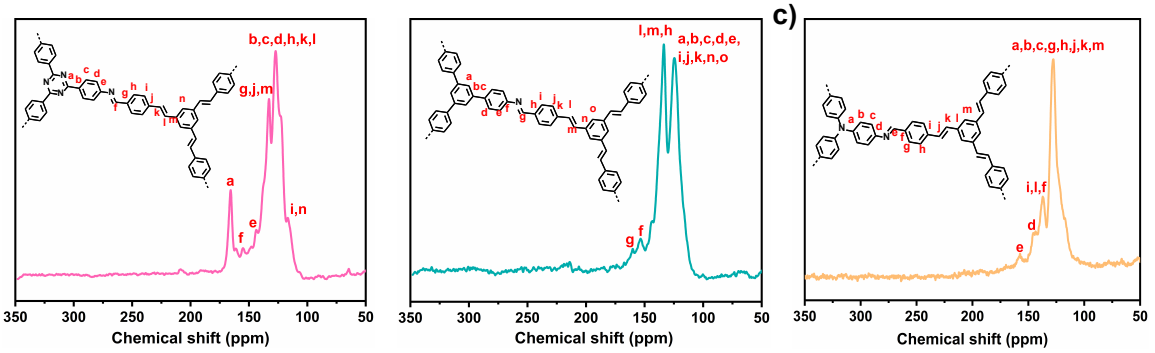

Figure S6. Solid-state ^{13}C NMR spectrum of a) OPV-TAPT-COF, b) OPV-TAPB-COF, and c) OPV-TAPA-COF.

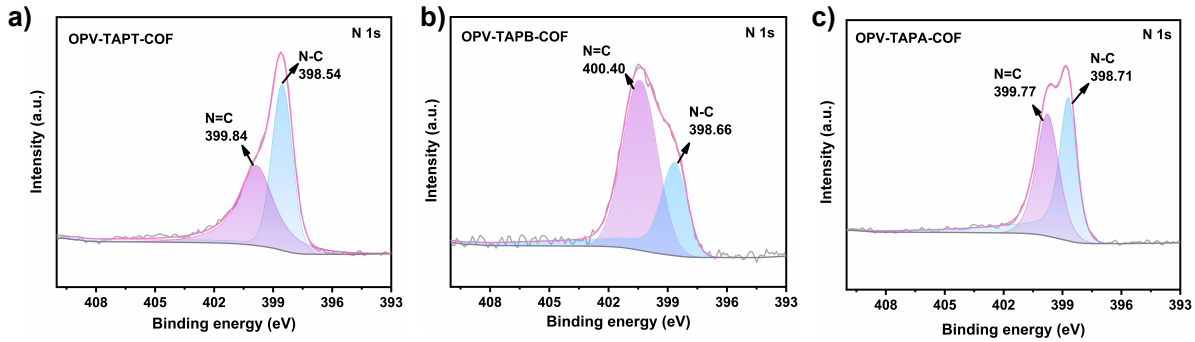

Figure S7. N 1s XPS spectra of a) OPV-TAPT-COF, b) OPV-TAPB-COF, and c) OPV-TAPA-COF.

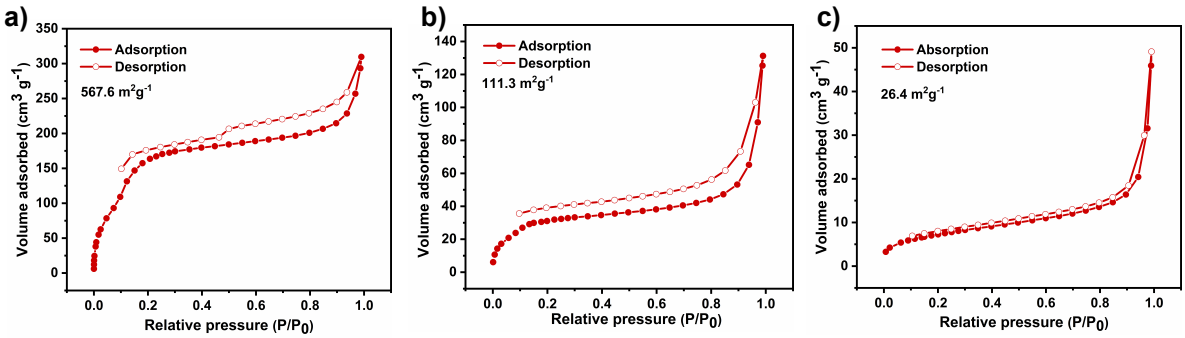

Figure S8. N_2 sorption isotherms for a) OPV-TAPT-COF, b) OPV-TAPB-COF, and c) OPV-TAPA-COF.

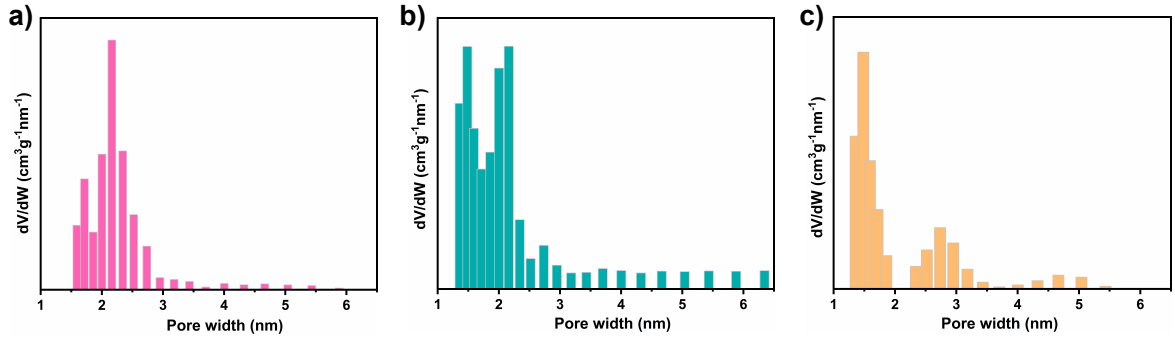

Figure S9. Pore size distributions for a) OPV-TAPT-COF, b) OPV-TAPB-COF, and c) OPV-TAPA-COF.

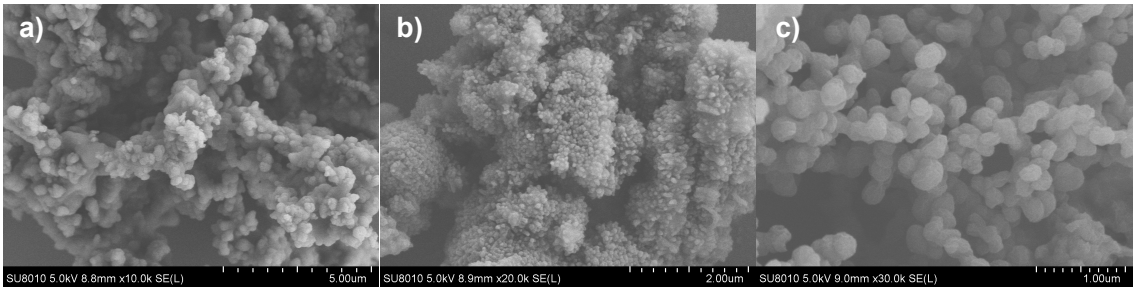

Figure S10. SEM images of a) OPV-TAPT-COF, b) OPV-TAPB-COF, and c) OPV-TAPA-COF.

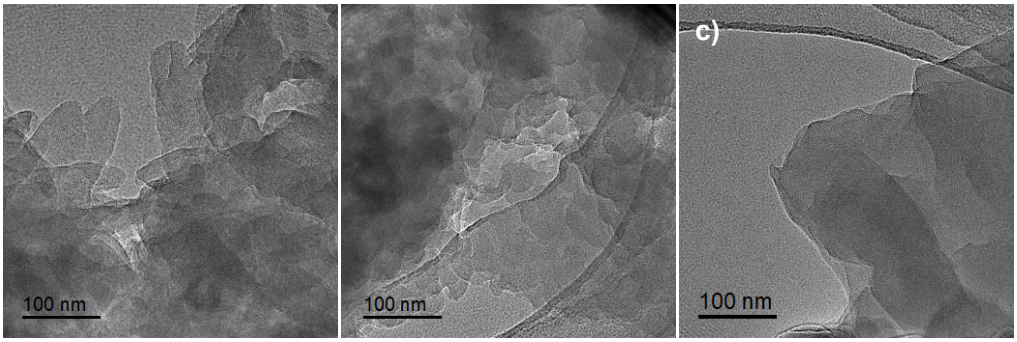

Figure S11. TEM images for a) OPV-TAPT-COF, b) OPV-TAPB-COF, and c) OPV-TAPA-COF.

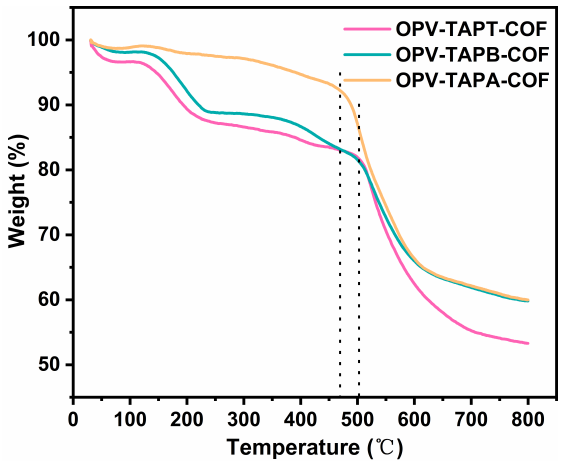

Figure S12. TGA curves of OPV-TAPT-COF, OPV-TAPB-COF, and OPV-TAPA-COF were recorded under a N_2 atmosphere.

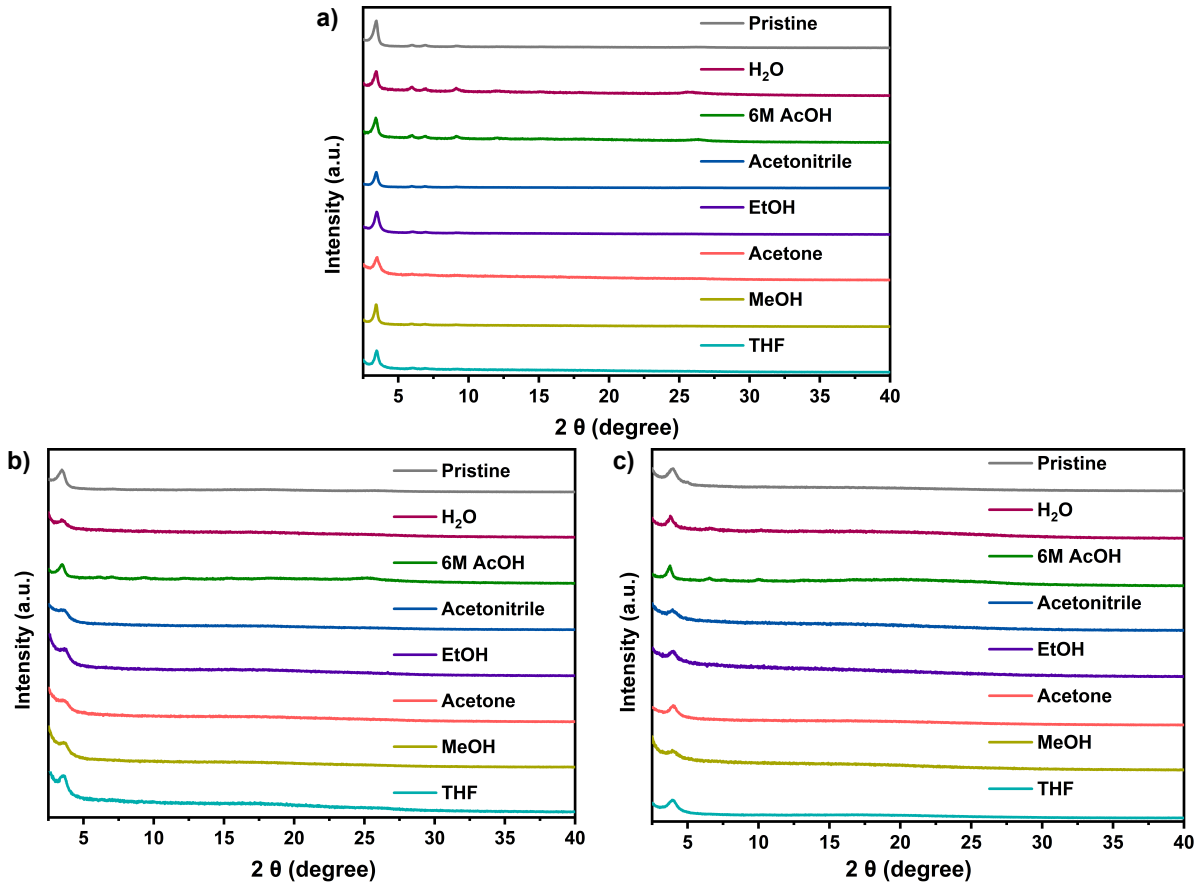

Figure S13. PXRD patterns of a) OPV-TAPT-COF, b) OPV-TAPB-COF, and c) OPV-TAPA-COF collected before and after immersion in different solvents for 24 h.

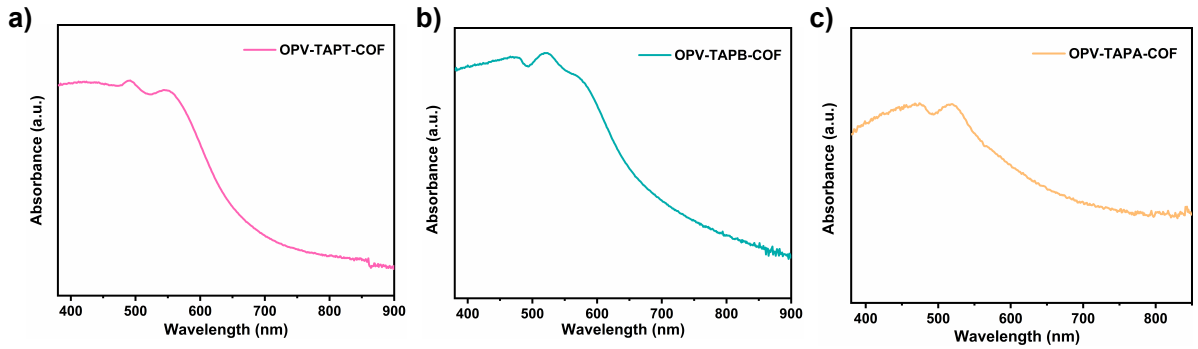

Figure S14. Solid-state UV-vis DRS spectrum of a) OPV-TAPT-COF, b) OPV-TAPB-COF, and c) OPV-TAPA-COF.

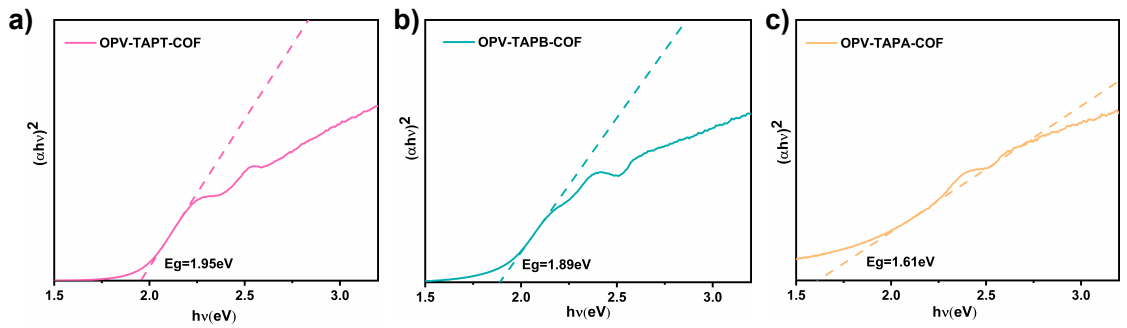

Figure S15. Tauc plots of a) OPV-TAPT-COF, b) OPV-TAPB-COF, and c) OPV-TAPA-COF.

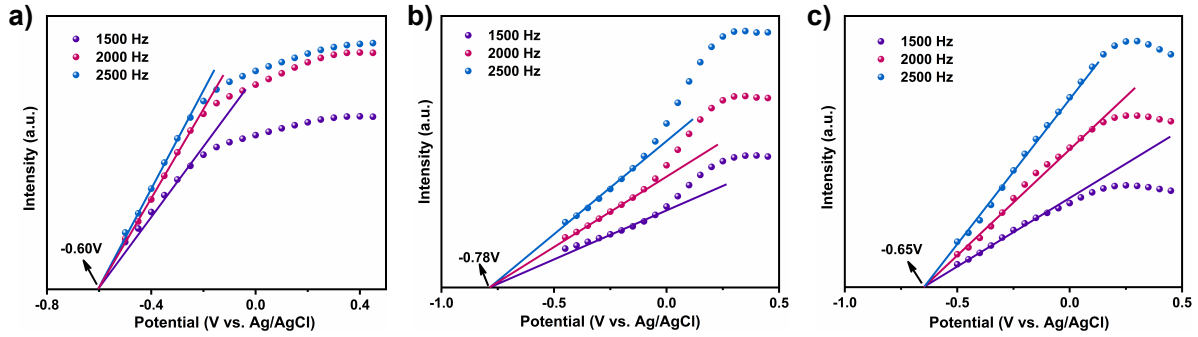

Figure S16. Mott-Schottky plots for a) OPV-TAPT-COF, b) OPV-TAPB-COF, and c) OPV-TAPA-COF.

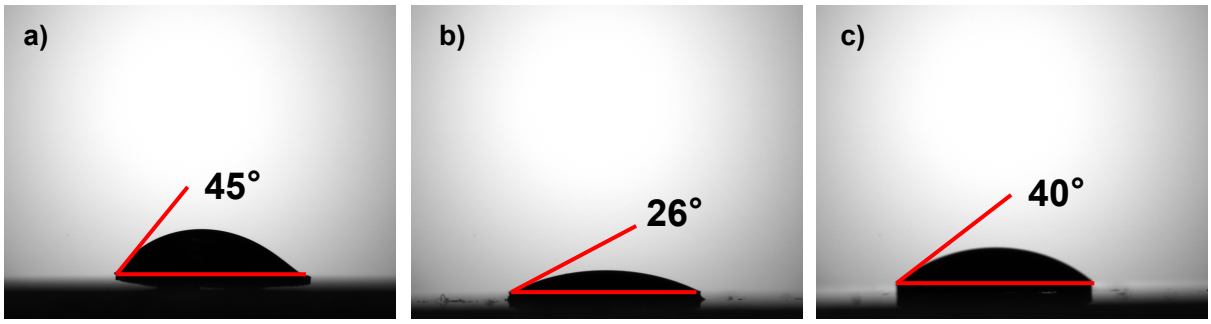

Figure S17. Water contact angles for pressed pellets of a) OPV-TAPT-COF, b) OPV-TAPB-COF, and c) OPV-TAPA-COF.

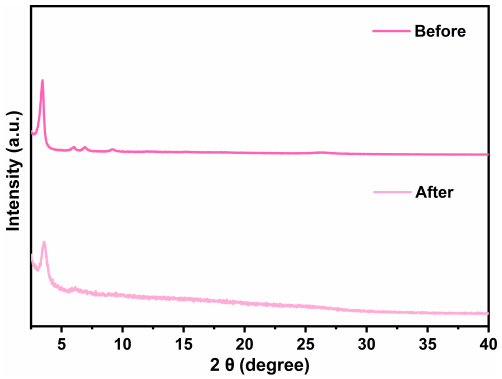

Figure S18. PXRD patterns of OPV-TAPT-COF before and after four consecutives photocatalytic H_2O_2 production cycles.

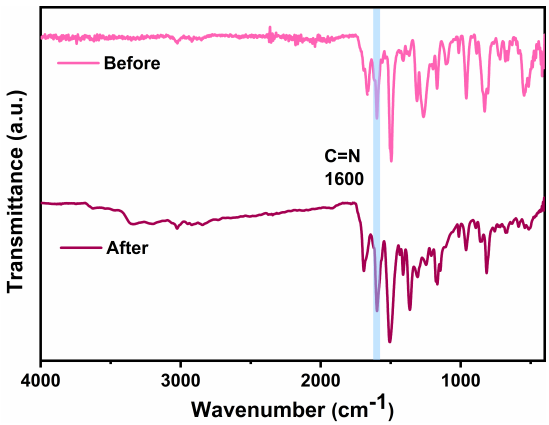

Figure S19. FT-IR spectra of OPV-TAPT-COF before and after four consecutives photocatalytic H_2O_2 production cycles.

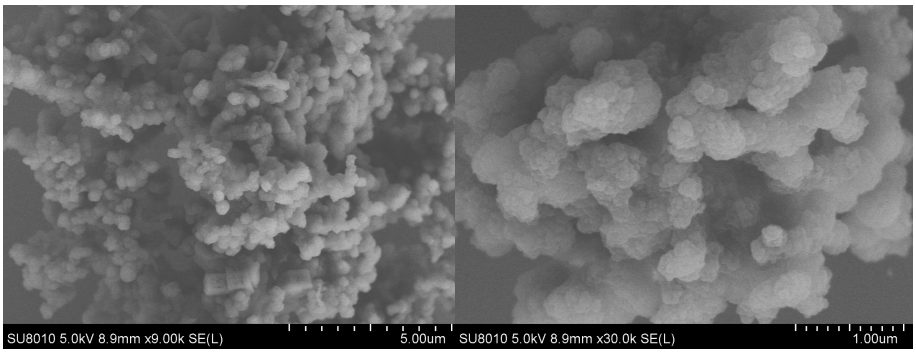

Figure S20. SEM pattern of OPV-TAPT-COF after four consecutives photocatalytic H_2O_2 production cycles.

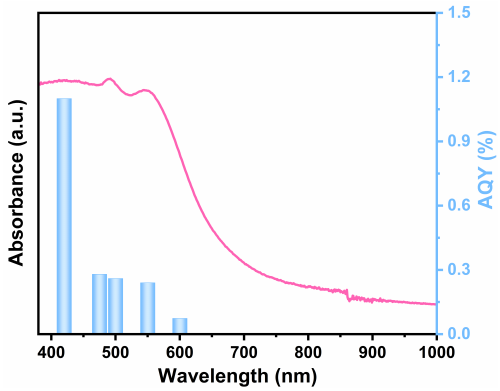

Figure S21. Wavelength-dependent AQY of H_2O_2 production for OPV-TAPT-COF.

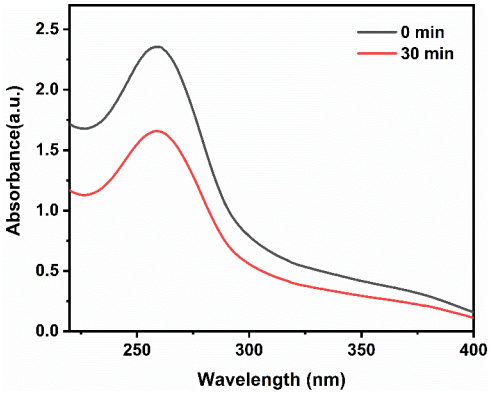

Figure S22. Detecting $\bullet O_2^-$ in the OPV-TAPT-COF photocatalytic systems by NBT.

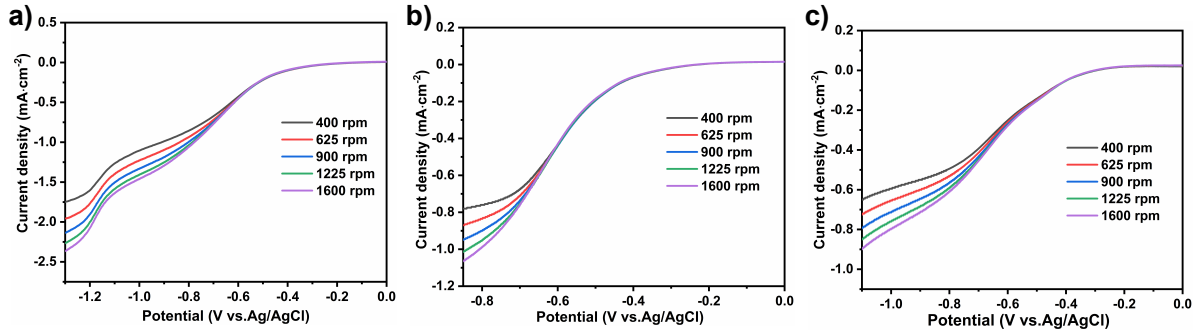

Figure S23. Linear sweep voltammograms at various rotation rates for a) OPV-TAPT-COF, b) OPV-TAPB-COF, and c) OPV-TAPA-COF.

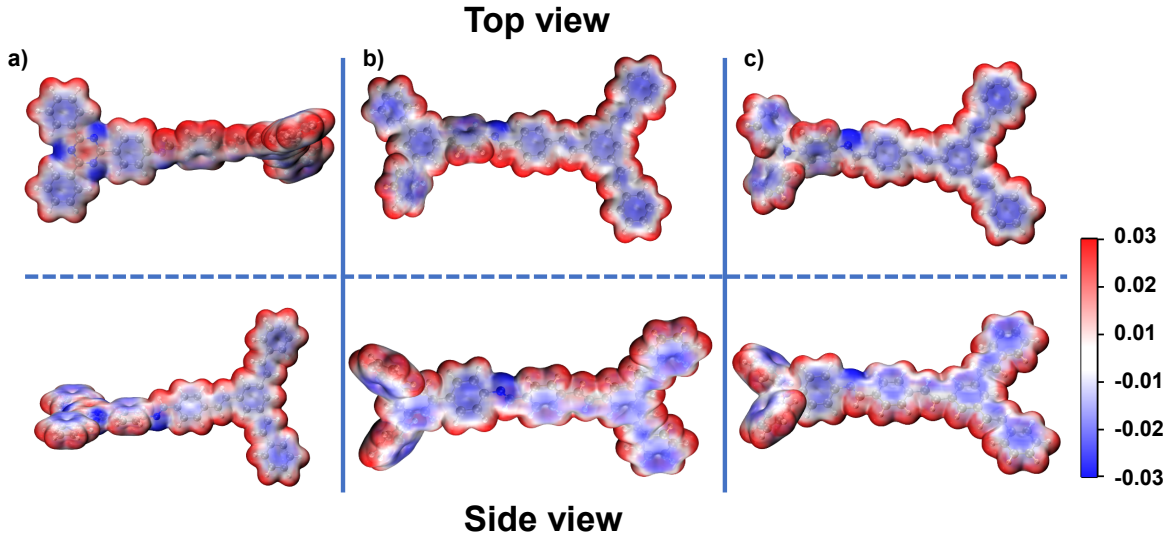

Figure S24. Electrostatic potential distribution of a) OPV-TAPT-COF, b) OPV-TAPB-COF, and c) OPV-TAPA-COF.

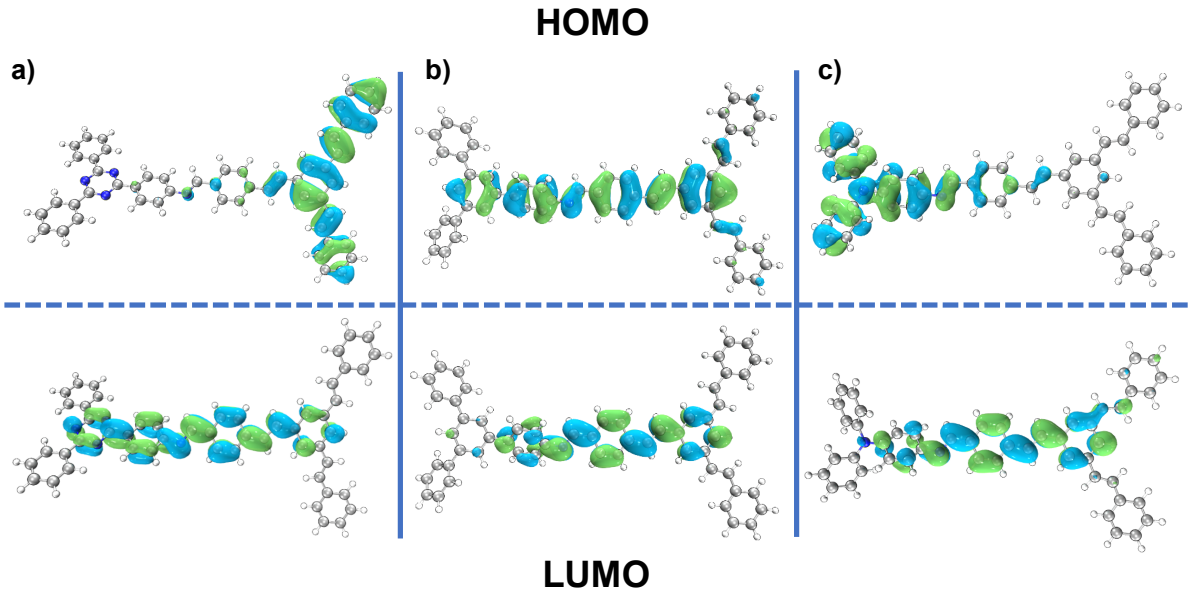

Figure 25. HOMO and LUMO orbital distribution on the fragment of a) OPV-TAPT-COF, b) OPV-TAPB-COF, and c) OPV-TAPA-COF.

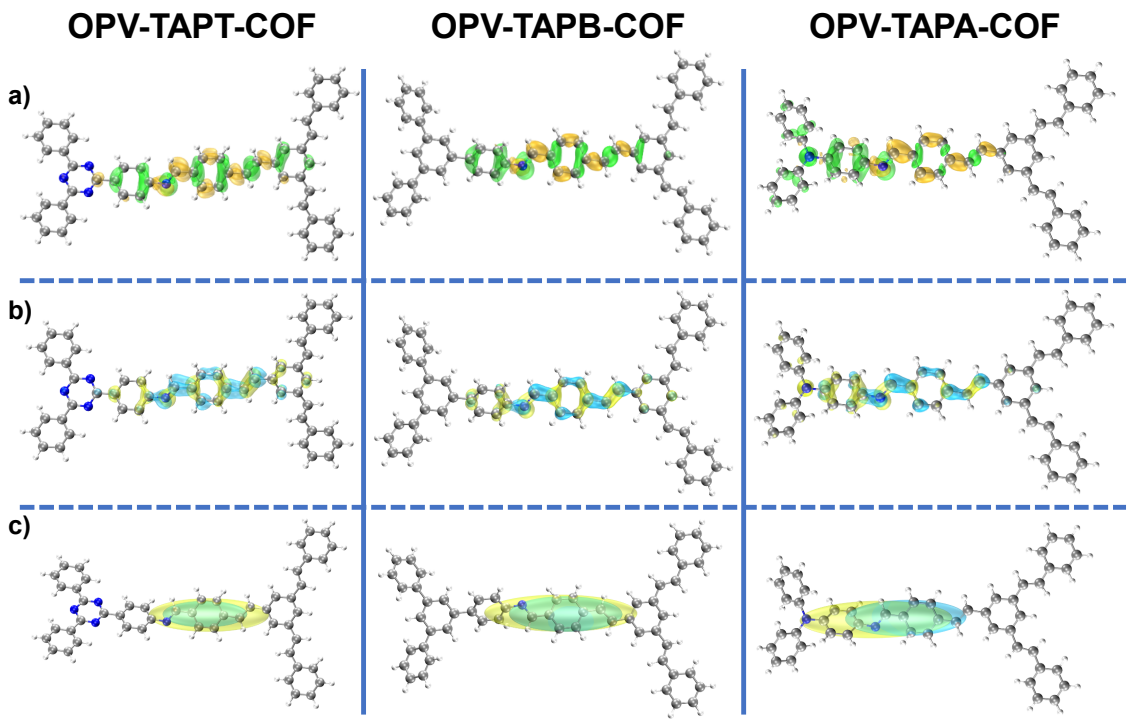

Figure 26. a) The charge density difference (CDD) plots (ISO:0.001; green: electron depletion; orange: electron accumulation), b) the electron-hole distribution isosurface schematic (ISO: 0.002; blue: electrons; yellow: holes), and c) the electron-hole distribution smoothing isosurface schematic (ISO: 0.0009; blue: electrons; yellow: holes) of OPV-TAPT-COF, OPV-TAPB-COF, and OPV-TAPA-COF.

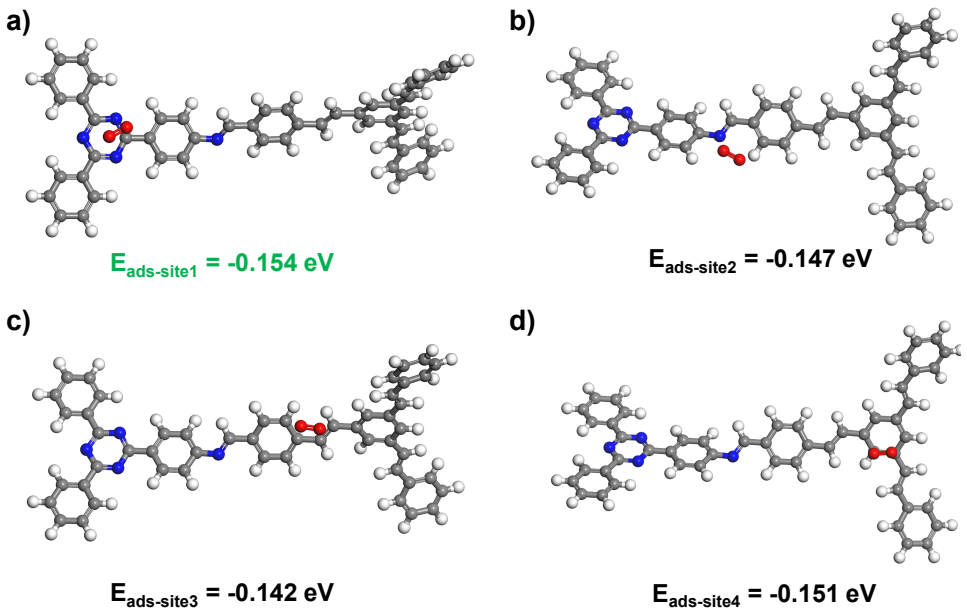

Figure S27. The structural diagram and adsorption energy of the possible O_2 adsorption sites of OPV-TAPT-COF(a) triazine site, b) imine site, c) vinylene site, d) phenyl carbon site).

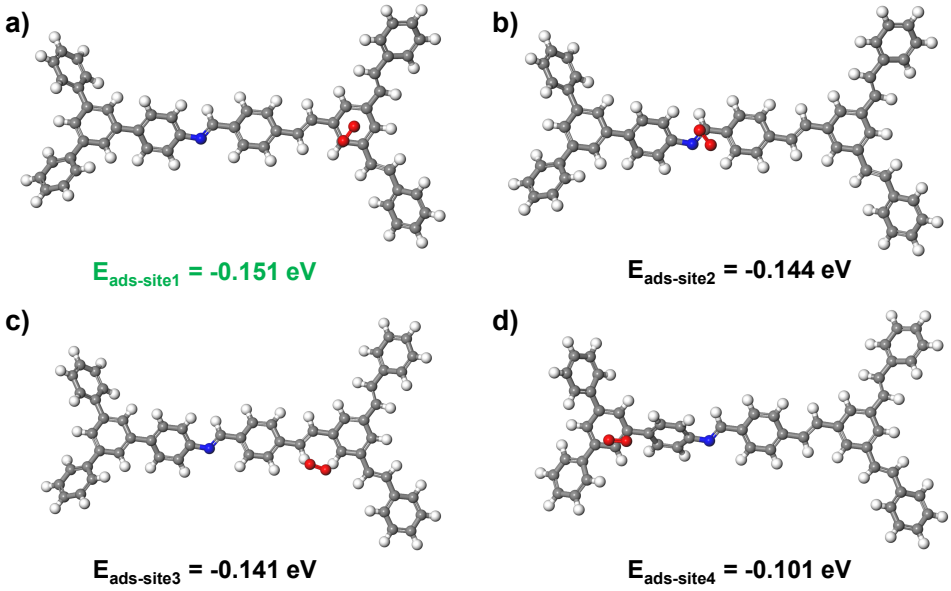

Figure S28. The structural diagram and adsorption energy of the possible O_2 adsorption sites of OPV-TAPB-COF(a)phenyl carbon site of the OPV unit, b) imine linkage site, c) hydrogen site, d) phenyl carbon site of the TAPB unit).

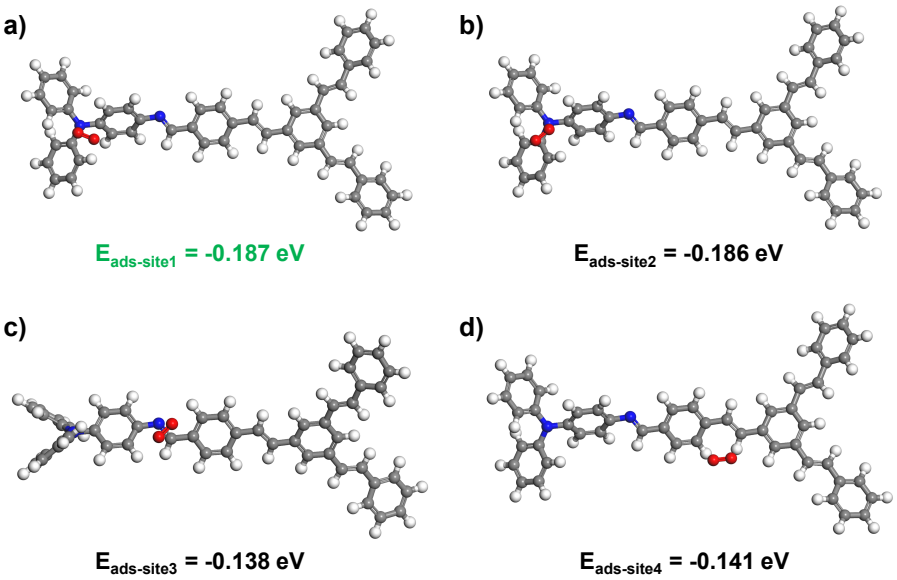

Figure S29. The structural diagram and adsorption energy of the possible O_2 adsorption sites of OPV-TAPA-COF(a) nitrogen site on the TAPB unit, with one oxygen atom of O_2 oriented toward a phenyl hydrogen, b) nitrogen site on the TAPB unit, c) imine linkage site, d) hydrogen site).

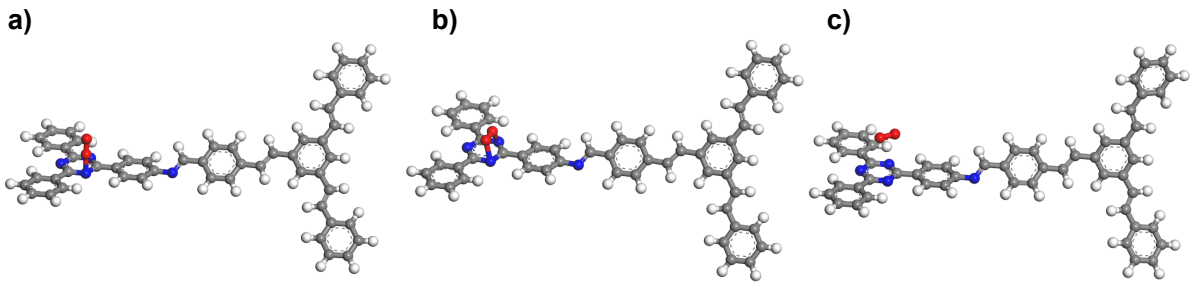

Figure S30. Two proposed adsorption modes of O_2 on OPV-TAPT-COF. a) Initial configuration for Pauling-type adsorption, b) initial configuration for Yeager-type adsorption, and c) the optimized adsorption configuration (Yeager-type).

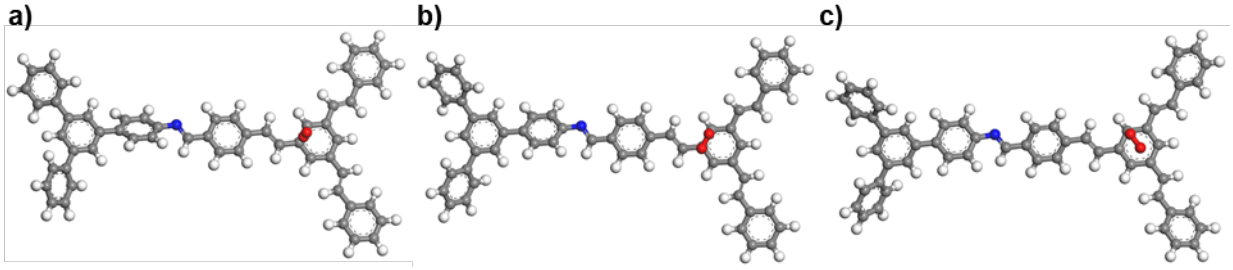

Figure S31. Two proposed adsorption modes of O_2 on OPV-TAPB-COF. a) Initial configuration for Pauling-type adsorption, b) initial configuration for Yeager-type adsorption, and c) the optimized adsorption configuration (Yeager-type).

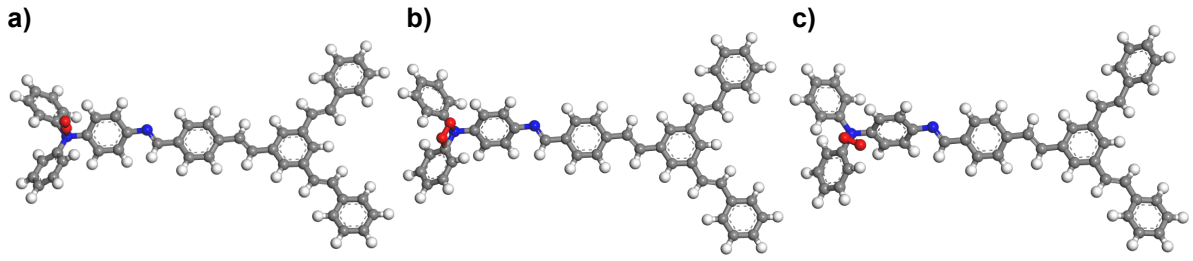

Figure S32. Two proposed adsorption modes of O_2 on OPV-TAPA-COF. a) Initial configuration for Pauling-type adsorption, b) initial configuration for Yeager-type adsorption, and c) the optimized adsorption configuration (Yeager-type).

7. Supplementary Tables

Table S1. The *Sr* index, hole delocalization index (*HDI*), electron delocalization index (*EDI*), and exciton binding energy (E_{coul}) were calculated for the three COFs.

COF	*Sr* (a.u.)	*HDI*	*EDI*	E_{coul} (eV)
OPV-TAPT-COF	0.81075	5.29	4.99	3.422711
OPV-TAPB-COF	0.80886	5.41	5.43	3.651934
OPV-TAPA-COF	0.75054	5.56	5.62	3.517562

Table S2. Unit cell parameters and fractional atomic coordinates for the unit cell of the OPV-TAPT-COF in eclipsed stacking (AA) mode.

Space group: P6 a=30.9814 Å, b=3.4533 Å, c=29.3835 Å α=γ=90° β= 120°			
Atom	x	y	z
C1	0.50183	0	-2.09582
C2	0.52378	0	-2.12786
C3	0.49437	0	-2.18233
C4	0.44209	0	-2.20631
C5	0.42048	0	-2.17403
C6	0.45001	0	-2.11947
C7	0.40854	0	-2.26416
C8	0.42423	0	-2.29942
C9	0.39138	0	-2.35736
C10	0.4143	0	-2.38838
C11	0.76739	0	-2.7021
N12	0.74328	0	-2.674
C13	0.66159	0	-2.83855

C14	0.6865	0	-2.86763
C15	0.65981	0	-2.92227
C16	0.60794	0	-2.94891
C17	0.58268	0	-2.92029
C18	0.60932	0	-2.86551
N19	0.98085	0	-2.60093
C20	0.54171	0	-2.59948
C21	0.06276	0	-2.59289
C22	0.08918	0	-2.53786
C23	0.14127	0	-2.51072
C24	0.16773	0	-2.53836
C25	0.14081	0	-2.59333
C26	0.08912	0	-2.62018
C27	0.22282	0	-2.513
C28	0.25462	0	-2.46111
C29	0.30989	0	-2.43711
C30	0.33905	0	-2.38225
C31	0.5314	0	-2.03793
C32	0.69274	0	-2.69887
N33	0.66657	0	-2.75209
C34	0.82239	0	-2.67583
C35	0.85183	0	-2.62096
C36	0.90376	0	-2.59712
C37	0.9273	0	-2.6274
C38	0.89763	0	-2.68241
C39	0.84602	0	-2.7061
N40	0.58942	0	-2.58147

C41	0.52071	0	-2.56408
C42	0.46903	0	-2.58587
C43	0.44756	0	-2.55388
C44	0.47751	0	-2.49884
C45	0.52942	0	-2.47719
C46	0.55088	0	-2.50939
C47	0.45682	0	-2.46254
C48	0.408	0	-2.47836
C49	0.38599	0	-2.44332
C50	0.33406	0	-2.46702
C51	0.00801	0	-2.62335
C52	0.69017	0	-2.78055
N53	0.74049	0	-2.7552
C54	0.66603	0	-2.6687
C55	0.61386	0	-2.6951
C56	0.58811	0	-2.66736
C57	0.61404	0	-2.61217
C58	0.66607	0	-2.58582
C59	0.69193	0	-2.61366
N60	0.58055	0	-3.00812
H61	0.56378	0	-2.11085
H62	0.51345	0	-2.20462
H63	0.38047	0	-2.19107
H64	0.43227	0	-2.09564
H65	0.36927	0	-2.27741
H66	0.46351	0	-2.28594
H67	0.45434	0	-2.36898

H68	0.72667	0	-2.84828
H69	0.67954	0	-2.94407
H70	0.54251	0	-2.94025
H71	0.58895	0	-2.84437
H72	0.51586	0	-2.64102
H73	0.06965	0	-2.51584
H74	0.16006	0	-2.46847
H75	0.15987	0	-2.61585
H76	0.06964	0	-2.66261
H77	0.23699	0	-2.53984
H78	0.24017	0	-2.43439
H79	0.32022	0	-2.35967
H80	0.56829	0	-2.03119
H81	0.83483	0	-2.59644
H82	0.92582	0	-2.55481
H83	0.91326	0	-2.70801
H84	0.82465	0	-2.74846
H85	0.44501	0	-2.62798
H86	0.40757	0	-2.57329
H87	0.55358	0	-2.43511
H88	0.59096	0	-2.49146
H89	0.48358	0	-2.42126
H90	0.38153	0	-2.51964
H91	0.31324	0	-2.50917
H92	-0.00867	0	-2.66541
H93	0.59262	0	-2.73747
H94	0.54811	0	-2.68991

H95	0.68669	0	-2.54343
H96	0.73213	0	-2.59204

Table S3. Unit cell parameters and fractional atomic coordinates for the unit cell of the OPV-TAPB-COF in eclipsed stacking (AA) mode.

Space group: P6 a=31.1279 Å, b=3.4516 Å, c=29.6643 Å α=γ=90° β= 120°			
Atom	x	y	z
C1	0.50013	0	-2.09858
C2	0.52202	0	-2.13037
C3	0.49296	0	-2.18412
C4	0.44109	0	-2.20765
C5	0.41953	0	-2.17564
C6	0.44871	0	-2.12178
C7	0.40793	0	-2.26475
C8	0.42367	0	-2.29964
C9	0.39127	0	-2.35683
C10	0.41424	0	-2.3875
C11	0.76892	0	-2.70326
C12	0.74302	0	-2.67529
C13	0.65948	0	-2.84355
C14	0.68331	0	-2.87395
C15	0.65661	0	-2.92786
C16	0.60541	0	-2.95376
C17	0.58067	0	-2.92518
C18	0.60709	0	-2.87111
N19	0.98374	0	-2.59925

C20	0.54088	0	-2.59738
C21	0.0657	0	-2.59027
C22	0.09133	0	-2.53593
C23	0.14303	0	-2.5088
C24	0.16983	0	-2.53579
C25	0.14368	0	-2.59006
C26	0.09242	0	-2.61688
C27	0.2245	0	-2.5105
C28	0.25573	0	-2.45925
C29	0.31062	0	-2.43551
C30	0.33933	0	-2.38135
C31	0.5294	0	-2.04144
C32	0.69099	0	-2.69976
C33	0.66502	0	-2.7544
C34	0.82514	0	-2.67616
C35	0.85462	0	-2.62147
C36	0.9062	0	-2.59724
C37	0.93057	0	-2.62614
C38	0.90209	0	-2.68027
C39	0.85083	0	-2.70458
N40	0.58818	0	-2.58011
C41	0.52019	0	-2.56206
C42	0.46893	0	-2.58323
C43	0.44766	0	-2.55137
C44	0.47739	0	-2.49706
C45	0.5289	0	-2.47601
C46	0.55016	0	-2.50809

C47	0.45684	0	-2.46098
C48	0.40838	0	-2.47641
C49	0.38636	0	-2.44172
C50	0.33484	0	-2.46507
C51	0.01143	0	-2.62081
C52	0.68866	0	-2.78452
C53	0.74055	0	-2.75772
C54	0.66378	0	-2.66873
C55	0.61157	0	-2.69336
C56	0.58648	0	-2.66524
C57	0.61231	0	-2.611
C58	0.66368	0	-2.58584
C59	0.68909	0	-2.61385
N60	0.57816	0	-3.01223
H61	0.56172	0	-2.11371
H62	0.51199	0	-2.20623
H63	0.37982	0	-2.19235
H64	0.43103	0	-2.09813
H65	0.36895	0	-2.27775
H66	0.46266	0	-2.28642
H67	0.45398	0	-2.36842
H68	0.76353	0	-2.63424
H69	0.72262	0	-2.8579
H70	0.67603	0	-2.94976
H71	0.54081	0	-2.94466
H72	0.58492	0	-2.85249
H73	0.51509	0	-2.6383

H74	0.0715	0	-2.51446
H75	0.16128	0	-2.46709
H76	0.16301	0	-2.61208
H77	0.07356	0	-2.65876
H78	0.23886	0	-2.53691
H79	0.24109	0	-2.43294
H80	0.32049	0	-2.35901
H81	0.566	0	-2.03497
H82	0.62602	0	-2.77386
H83	0.83927	0	-2.59596
H84	0.92739	0	-2.55541
H85	0.91844	0	-2.70498
H86	0.83298	0	-2.74604
H87	0.44506	0	-2.62477
H88	0.408	0	-2.57035
H89	0.55287	0	-2.4345
H90	0.58992	0	-2.49066
H91	0.48333	0	-2.42025
H92	0.3822	0	-2.51713
H93	0.31439	0	-2.50667
H94	-0.00444	0	-2.66228
H95	0.75896	0	-2.77963
H96	0.58822	0	-2.73458
H97	0.54678	0	-2.687
H98	0.68435	0	-2.54399
H99	0.7286	0	-2.59095

Table S4. Unit cell parameters and fractional atomic coordinates for the unit cell of the OPV-TAPA-COF in eclipsed stacking (AA) mode.

Space group: P1 a=4.0574 Å, b=27.9525 Å, c=27.1053 Å α=120° β=γ=90°			
Atom	x	y	z
N1	-0.37234	3.51075	1.26303
C2	-0.35414	3.48108	1.20111
C3	-0.51413	3.50098	1.16863
C4	-0.49062	3.47336	1.10957
C5	-0.31169	3.42451	1.0812
C6	-0.15105	3.404	1.11271
C7	-0.17235	3.43204	1.17181
C8	-0.37724	3.48066	1.29456
C9	-0.50738	3.42701	1.27047
C10	-0.52017	3.39871	1.30087
C11	-0.40274	3.42335	1.35686
C12	-0.26544	3.4759	1.38079
C13	-0.25324	3.50417	1.35032
C14	-0.3918	3.57077	1.29299
C15	-0.57556	3.59964	1.34325
C16	-0.60224	3.65692	1.37106
C17	-0.4489	3.68706	1.3485
C18	-0.26381	3.65885	1.29889
C19	-0.23339	3.60175	1.2718
N20	-0.28515	3.39748	1.02052
N21	-0.47505	3.74577	1.37364
N22	-0.41297	3.39657	1.39057

C23	-0.55831	4.32826	1.41686
C24	-0.57125	4.35168	1.37856
C25	-0.71147	4.27768	1.40047
C26	-0.70293	4.25437	1.43572
C27	-0.5414	4.28152	1.48863
C28	-0.38816	4.33223	1.5048
C29	-0.39613	4.3554	1.4694
C30	-0.52174	4.2589	1.52806
C31	-0.67535	4.21307	1.52009
C32	-0.64465	4.19125	1.55984
C33	-0.67934	4.13448	1.5385
C34	-0.65429	4.11179	1.57454
C35	-0.6057	4.14695	1.63272
C36	-0.57222	4.204	1.65502
C37	-0.5947	4.22583	1.61833
C38	-0.53642	4.24209	1.71675
C39	-0.40357	4.22689	1.7523
C40	-0.3947	4.26178	1.81503
C41	-0.23389	4.24106	1.84653
C42	-0.23926	4.27001	1.90577
C43	-0.40467	4.32028	1.93458
C44	-0.56088	4.34187	1.9037
C45	-0.55655	4.31298	1.84447
C46	-0.68679	4.05197	1.5537
C47	-0.62664	4.01319	1.49995
C48	-0.64086	3.95328	1.47972
C49	-0.48284	3.9173	1.42856

C50	-0.48335	3.86065	1.40819
C51	-0.6444	3.8387	1.43849
C52	-0.80865	3.87435	1.48896
C53	-0.80849	3.93105	1.50936
C54	-0.64433	3.77906	1.41819
C55	-0.43068	4.34872	1.99777
H56	-0.65486	3.53833	1.1887
H57	-0.61403	3.48986	1.08577
H58	-0.00916	3.36639	1.09155
H59	-0.04947	3.41492	1.19452
H60	-0.59449	3.40585	1.2275
H61	-0.61865	3.35748	1.27968
H62	-0.17041	3.4954	1.42368
H63	-0.15342	3.54507	1.37143
H64	-0.69902	3.57801	1.36135
H65	-0.74675	3.67664	1.40944
H66	-0.14195	3.68134	1.28105
H67	-0.08995	3.58194	1.2336
H68	-0.83854	4.25604	1.36017
H69	-0.82338	4.21521	1.42071
H70	-0.26009	4.354	1.54498
H71	-0.27454	4.39444	1.48315
H72	-0.36735	4.28097	1.56515
H73	-0.8208	4.18894	1.4825
H74	-0.72982	4.10842	1.4938
H75	-0.60144	4.12953	1.66061
H76	-0.58066	4.26994	1.63586

H77	-0.62082	4.28373	1.73239
H78	-0.29693	4.18625	1.73482
H79	-0.1074	4.20187	1.82523
H80	-0.11805	4.25285	1.92915
H81	-0.69391	4.3804	1.92556
H82	-0.68979	4.33046	1.82267
H83	-0.7416	4.03992	1.58507
H84	-0.54319	4.02537	1.46985
H85	-0.35345	3.93315	1.40468
H86	-0.35529	3.83416	1.36897
H87	-0.9391	3.85828	1.51253
H88	-0.94516	3.95681	1.54768
H89	-0.78759	3.76406	1.44135
H90	-0.69568	0.3528	-0.99061
H91	-0.71913	0.33072	-0.6594

Table S5. The photocatalytic H_2O_2 performance of OPV-TAPT-COF and comparison with recently reported COF-based photocatalysts.

Samples	H_2O_2 Production ($\mu mol\ g^{-1}\ h^{-1}$)	Light source	Reactant solution	Ref.
OPV-TAPT-COF	3094	$\lambda > 420$ nm	H_2O/Air	This work
OPV-TAPT-COF	1176	Sunlight	H_2O/Air	This work
BTZ-1	1140	$\lambda > 420$ nm	H_2O:BA=9:1/O_2	[11]
BTZ-3	3267	$\lambda > 420$ nm	H_2O:BA=9:1/O_2	
BTZ-3	650	$\lambda > 420$ nm	H_2O/O_2	
BBT-ACN COF-1	2500	$\lambda > 420$ nm	H_2O/Air	[12]
BBT-ACN COF-2	910	$\lambda > 420$ nm	H_2O/Air	
ECUT-COF-95	2012	$\lambda \geq 400$ nm	H_2O/Air	[13]
ECUT-COF-96	2575	$\lambda \geq 400$ nm	H_2O/Air	
TpPy	1615.5	$\lambda > 420$ nm	H_2O/O_2	[14]
TpPh	400.3	$\lambda > 420$ nm	H_2O/O_2	
BcPy	544.8	$\lambda > 420$ nm	H_2O/O_2	
BTT-DTA-COF	1621	LED (400-700 nm)	H_2O/Air	[15]
BTT-BAT-COF	1942	LED (400-700 nm)	H_2O/Air	
BTT-TTA-COF	2078	LED (400-700 nm)	H_2O/Air	

TTA-BT-COF	3009	LED (400-700 nm)	H_2O/Air	
TTA-TF-COF	3343	LED (400-700 nm)	H_2O/Air	
N_0-COF	1529	λ > 420 nm	H_2O/O_2	[16]
N_1-COF	2980	λ > 420 nm	H_2O/O_2	
N_2-COF	3341	λ > 420 nm	H_2O/O_2	
N_3-COF	4881	λ > 420 nm	H_2O/O_2	
TPB–TPT-COF	6740	λ > 420 nm	H_2O/O_2	[17]
TPB-COF	2030	λ > 420 nm	H_2O/O_2	
sp^2 c-CTF-4@AB	2758	Blue LED	H_2O/O_2	[18]
sp^2 c-CTF-4@AA	1020	Blue LED	H_2O/O_2	
COF-920-1N	4288	λ > 420 nm	H_2O/Air	[19]
COF-920-0N	3435	λ > 420 nm	H_2O/Air	
COF-920-3N	2218	λ > 420 nm	H_2O/Air	
TpBa	808.8	λ > 400 nm	H_2O/Air	[20]
TpDa	686.4	λ > 400 nm	H_2O/Air	
TpPa	416.1	λ > 400 nm	H_2O/Air	
BT-COF	4524	λ > 420 nm	H_2O/Air	[21]
BP-COF	932	λ > 420 nm	H_2O/Air	
BA-COF	304	λ > 420 nm	H_2O/Air	
A-COF	1155.5	λ ≥ 400 nm	H_2O/O_2	[22]
H-COF	400	λ ≥ 400 nm	H_2O/O_2	
I-COF	304	λ ≥ 400 nm	H_2O/O_2	

8. Supplementary References

1. W. Dong, Z. Qin, K. Wang, Y. Xiao, X. Liu, S. Ren and L. Li, *Angew. Chem., Int. Ed.*, 2022, **62**, e202216073.
2. Y. Zhang, C. Pan, G. Bian, J. Xu, Y. Dong, Y. Zhang, Y. Lou, W. Liu and Y. Zhu, *Nat. Energy.*, 2023, **8**, 361.
3. M. J. Frisch, G. W. Trucks, H. B. Schlegel, G. E. Scuseria, M. A. Robb, J. R. Cheeseman, G. Scalmani, V. Barone, G. A. Petersson, H. Nakatsuji, X. Li, M. Caricato, A. V. Marenich, J. Bloino, B. G. Janesko, R. Gomperts, B. Mennucci, H. P. Hratchian, J. V. Ortiz, A. F. Izmaylov, J. L. Sonnenberg, Williams, F. Ding, F. Lipparini, F. Egidi, J. Goings, B. Peng, A. Petrone, T. Henderson, D. Ranasinghe, V. G. Zakrzewski, J. Gao, N. Rega, G. Zheng, W. Liang, M. Hada, M. Ehara, K. Toyota, R. Fukuda, J. Hasegawa, M. Ishida, T. Nakajima, Y. Honda, O. Kitao, H. Nakai, T. Vreven, K. Throssell, J. A. Montgomery Jr., J. E. Peralta, F. Ogliaro, M. J. Bearpark, J. J. Heyd, E. N. Brothers, K. N. Kudin, V. N. Staroverov, T. A. Keith, R. Kobayashi, J. Normand, K. Raghavachari, A. P. Rendell, J. C. Burant, S. S. Iyengar, J. Tomasi, M. Cossi, J. M. Millam, M. Klene, C. Adamo, R. Cammi, J. W. Ochterski, R. L. Martin, K. Morokuma, O. Farkas, J. B. Foresman and D. J. Fox, *Journal*, 2016.
4. A. D. Becke, *Phys. Rev.*, 1988, **38**, 3098.
5. P. J. Stephens, F. J. Devlin, C. F. Chabalowski and M. J. Frisch, *J. Phys. Chem.*, 1994, **98**, 11623-11627.
6. S. Grimme, J. Antony, S. Ehrlich and H. Krieg, *J. Chem. Phys.*, 2010, **132**, 154104.
7. A. D. Becke, *J. Chem. Phys.*, 1993, **98**, 1372.
8. C. Lee, W. Yang and R. G. Parr, *Phys. Rev.*, 1988, **37**, 785.
9. T. Lu and F. Chen, *J Comput Chem.*, 2011, **33**, 580.
10. W. Humphrey, A. Dalke and K. Schulten, *J. Mol. Graph. Model.*, 1996, **14**, 33.
11. Y. Wang, X. Zhao, G. Han, J. Bi and Y. Zhao, *Adv. Funct. Mater.*, 2025, DOI: 10.1002/adfm.202508550.
12. X. Wang, H. Li, S. Zhou, J. Ning, H. Wei, X. Li, S. Wang, L. Hao and D. Cao, *Adv. Funct. Mater.*, 2025, **35**, 242035.
13. H. Ren, Y. Liu, Z. Huang, L. Guo and F. Luo, *Chem. Commun.*, 2025, **61**, 8443.
14. Q. Liao, Z. Li, Q. Sun, H. Xu, Y. Wang, Y. Xu, H. Wu, Z. Zhang, Y. Xie, H. Li, D. Wang, G. Li and K. Xi, *ACS Appl. Nano Mater.*, 2025, **8**, 8095.
15. X. Yang, Z. X. Pan, J. Y. Yue, X. Li, G. Liu, Q. Xu and G. Zeng, *Small.*, 2024, **20**, 2405907.
16. Y. Zhang, Y. Wu, H. Ma, Y. Gao, X. Fan, Y. Zhao, F. Kang, Z. Li, Y. Liu and Q. Zhang, *Small.*, 2025, **21**, 2500674.
17. L. Li, X. Yao, W. Ou, J. Chai, R. Ma, C. Ran, A. Ma, X. Shi, P. Wei, H. Dong, H. Zhou, W. Yang, H.-C. Hu, J.-F. Wu, H. Peng and G. Ma, *Green Chem.*, 2025, **27**, 9144.
18. Q. Xie, A. Chen, X. Li, C. Xu, S. Bi, W. Zhang, J. Tang, C. Pan, F. Zhang and G. Yu, *Chem. Sci.*, 2025, **16**, 2215.
19. W. Dong, Z. Qin, X. Liu and L. Li, *Chin. J. Chem.*, 2025, **43**, 1504.
20. L. Wang, D. Ma, A. Liu, H. Du, Y. Fu, A. M. Al-Enizi, A. Nafady, S. Ma and Q. Wang, *Angew. Chem., Int. Ed.*, 2025, DOI: 10.1002/anie.202518097.
21. K. Xiong, X. Jia, Y. Kong, J. Yang, J. Guo, S. Li, M. Adeli, Y. Wang, X. Luo, X. Han and C. Cheng, *Adv. Funct. Mater.*, 2025, DOI: 10.1002/adfm.202510257.
22. S. Yang, D. Si, L. Zou, M. Shi, Y. Huang and R. Cao, *J. Am. Chem. Soc.*, 2025, **147**, 30287.